New Physics: Sae Mulli,
Vol. 72, No. 2, February 2022, pp. 90∼95
http://dx.doi.org/10.3938/NPSM.72.90

Photoluminescence Signatures of Subband-specific Mobility Spectrum in Two-dimensional Electron gas System

I. H. Ahn
Quantum-Functional Semiconductor Research Center, Dongguk University, Seoul 04620, Korea

H. Y. Hwang · Y. D. Jho*
School of Electrical Engineering and Computer Science,
Gwangju Institute of Science and Technology, Gwangju 61005, Korea

(Received 26 April 2021 : accepted 14 December 2021)

In this paper, we investigated a subband-specific relationship between electron mobility and photoluminescence (PL) intensity in a modulation-doped $In_{0.53}Ga_{0.47}As/In_{0.52}Al_{0.48}As$ heterostructure. From the steady-state diffusion model, the temperature-dependent mobility variation was anticipated to be inversely proportional to the PL intensity under lateral diffusion. The subband-mobility ratio fits best with the inverse ratio of the subband-specific PL intensity, especially in the high-temperature region ($\geq$100 K), where the carrier mobility is less influenced by carrier localization using alloy disorder. Furthermore, the localization effects were manifested by an abrupt increase in PL decay time at the vicinity of electron de-trapping temperature, which coincides with abrupt changes in thermally stimulated capacitance.

Keywords: Mobility spectrum analysis, Two-dimensional electron gas, Fermi-edge singularity, Photoluminescence

I. Introduction

Electron mobility is a fundamental parameter governing transport properties in semiconductor devices incorporating a two-dimensional electron gas (2DEG). Thus, reliable approaches for extracting mobilities have become of central interest in semiconductor science [1]. Conventional mobility measurement techniques using the Van der Pauw method or Hall bar-shaped patterns are unsuitable for determining the 2DEG mobility in doped heterostructures due to the presence of several parallel conducting layers. Instead, a combined mobility model, such as the two-layer [2] or three-layer models [3] has been used to interpret Hall measurements. Particularly, Shubnikov-de Haas analysis [4] and mobility spectrum analysis (MSA) [5] via magnetoresistance effect have led to an in-depth understanding of the mobility and relaxant transport properties of of 2DEG. With regard to optical properties, 2DEG has made features of many-body interaction such as Fermi-energy edge singularity (FES) [6,7] and bandgap renormalization [8].

Among various optical methodologies, photoluminescence (PL) has been correlated with the diffusion length in earlier works on bulk semiconductors [9] and in recent studies on organic materials [10], carbon nanostructures [11], nanoscale compound semiconductors [12], and polycrystals [13]. Moreover, a comparative study between electrical properties and PL spectra has been conducted at fixed temperatures in InGaAs-based structures for 2DEG [14, 15]. However, studies on optical signatures of subband-specific mobilities have been limited and PL properties have not been correlated with mobilities within the framework of temperature dependence. Motivated by the importance of electronic mobilities for recombination efficiency and transport in 2DEG

*E-mail: jho@gist.ac.kr

This is an Open Access article distributed under the terms of the Creative Commons Attribution Non-Commercial License (http://creativecommons.org/licenses/by-nc/3.0) which permits unrestricted non-commercial use, distribution, and reproduction in any medium, provided the original work is properly cited.

systems, we investigated a temperature-dependent correlation between mobility values and PL intensity from a specific quantum well (QW) subbands.

II. Experimental Schemes

An $In_{0.53}Ga_{0.47}As/In_{0.52}Al_{0.48}As$ heterostructure was grown by molecular beam epitaxy, consisting of a 500-nm-thick In $In_{0.52}Al_{0.48}As$ buffer layer on an InP substrate, 12-nm-thick undoped $In_{0.53}Ga_{0.47}As$, 4-nm-thick spacer of undoped $In_{0.52}Al_{0.48}As$, delta-doped sheet of Si ($4.5 \times 10^{12}cm^{-2}$), 20-nm-thick undoped $In_{0.52}Al_{0.48}As$, and 5-nm-thick cap layer of n-doped $In_{0.53}Ga_{0.47}As$ to assist in ohmic contact formation for MSA [16]. CW PL spectra were obtained using an Ar-ion laser (centered at 514.5 nm) at the excitation power I_{ex} of ∼50 W/cm^2 to be traced over a broad temperature range and compared with subband-specific mobilities. To characterize the temperature dependence of the electron-hole recombination, time-resolved PL experiments were conducted under excitation of picosecond diode laser (centered at 634 nm) using time-correlated single-photon counting (TCSPC) system. To probe specific energy states, the PL was spectrally filtered by a monochromator with a spectral window of 3 meV. Results showed that the instrumental resolution of TCSPC (∼ 50 ps) was better than the excitation pulse width (∼ 100 ps), therefore, much shorter than the rise time (≥ 500 ps) or decay time scale (≥ 1 ns) at the main peaks of the sample (Cf. Fig. 2(b) and 4).

Mobilities were compared with PL features as a function of temperatures from 10 to 290 K. The electron sheet carrier density was 3.33×10^{12} cm^{-2} determined from the hall measurements at 10 K. The simulated subband structure using self-consistent Schrödinger–Poisson equations reveals that the first and second electron subbands E_1 and E_2 are located below the Fermi-energy level of the 2DEG (E_F) in our doping density in Fig. 1(a). The interband-transition energies between electronic subbands (E1 and E2) and the first heavy-hole band (H1) are represented by the differently colored vertical arrows in conjunction with the corresponding wavefunctions. From the asymmetric potential profile, the electron transition between the first electronic subband

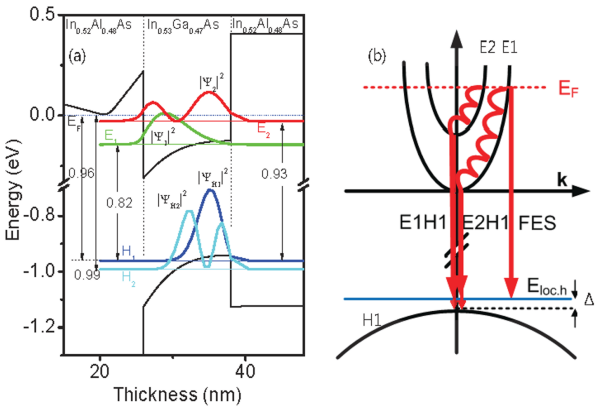

Fig. 1. (Color online) (a) Conduction and valence band profiles with squared envelope functions for electrons ($|\Psi_1|^2$, $|\Psi_2|^2$) and holes ($|\Psi_{H1}|^2$, $|\Psi_{H2}|^2$). (b) Optical recombination scheme for transitions from first and second subbands to localized state ($E_{loc.h}$) and/or heavy-hole subband (E1H1, E2H1) and from Fermi-energy level to localized state (FES).

and H1 (E1H1) [17–20], and the transition between the second subband and H1 (E2H1) are optically allowed as cartooned in the energy-momentum dispersion of Fig. 1(b). The vertical transition denoted as FES refers to the Fermi-energy edge singularity, ascribed to the enhanced oscillator strength at the Fermi-energy via many-body effects [6,21,22] between 2DEG and photo-carriers. The electrons at the Fermi energy recombine without k-restriction due to hole localization in the disordered system [21]. The deviation between H1 and $E_{loc,h}$, denoted by Δ, was caused by the localization of holes on various defects [23], whereas the electronic localization with shallow trapping energies was not included in Fig. 1(b). Here, we ignore the contribution of light holes and consider only the heavy-hole subbands, because the intrinsic compressive strain of the InGaAs QW relieves the degeneracy between the light and heavy-hole bands and sets the light hole subband at least 50 meV above [27].

Figure 2 shows the temperature dependence of PL spectra in (a) spectral-domain and in (b) time-domain with increasing temperatures. The three main peaks were resolved at the low T region and assigned to E1H1, E2H1, and FES, respectively, where I_{E1H1}, I_{E2H1}, and I_{FES} were the maximum intensity values in a PL spectrum. The width of the PL band at 10 K in Fig. 2(a) was broadened from the lowest E1H1 to FES.

The PL peak separation between E1H1 and FES was roughly 4 meV larger than the simulated Fermi energy

($= E_F - E_1$) in Fig. 1(a), due to the ignored effects of the exchange-correlation, non-parabolicity, hole localization effects, and additional photo-carrier population in this simplified calculation of 2DEG. The peak energies similarly followed the phenomenological Varshini formula for E1H1 and E2H1, contrary to the reduced redshift for the highest FES peak. These phenomena can be explained as follows: The FES peak energy was initially decreasing similarly to E1H1, as in Fig. 2(a), from 10 − 100 K. Above 100 K, thermally activated donor electrons transited to E1 states, increasing the first subband carrier density nE 1 and resulting in larger $E_F - E_1 \sim \pi\hbar^2 n_{E_1}/m^*$, where $\hbar$ is the Planck constant and m^* is the effective mass. Such effects were observed at E_1 state as the n_{E_1} measured from MSA rapidly increased at temperature T above 100 K. However, the carrier density in E_2 state slightly decreased with T elevating in MSA, thereby increasing $E_F - E_2$ above 100 K, as shown in Fig. 2(a) [16]. Above 100 K, $I_{\rm FES}$ was rapidly suppressed as holes were delocalized from traps near the alloy disorders. Time-resolved (TR) PL measurements were performed on the three main peaks, as in Fig. 2(a), and are representatively shown for E1H1 in Fig. 2(b). TR-PL lineshapes can be fitted using simple phenomenological biexponential decay responses:

$$I_{PL} = [1 - e^{-t/\tau_r}][I_1 e^{-t/\tau_1} + I_2 e^{-t/\tau_2}], \qquad (1)$$

where t is the time delay, τ_r is the rise time, and $\tau_1(\tau_2)$ are decay times with $I_1 > I_2$. τ_r was settled about 0.8 ns whereas τ_1 and τ_2 were non-monotonically changing between 0.6 and 20 ns with temperatures (specific values are discussed in later parts for all the three main peaks along with Fig. 4). Note that the characteristic time scales in Fig. 2(b) are much larger than the electronic diffusion time scale $t_\alpha = 1/\alpha^2 D$ (<1 ps, with the absorption depth $1/\alpha$ on the order of 200 nm [25] and diffusion coefficient D about 250 cm^2/s [26] or the momentum relaxation time scale T_2, estimated to be less than 2 ps in our temperature range, considering the homogeneous emission linewidth of 1.9 meV and the temperature-dependent electron-phonon scattering rates measured in undoped structures [27]. Therefore, PL emission appeared after carriers were stabilized

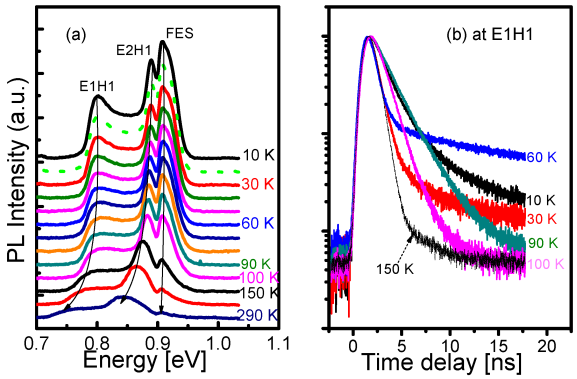

Fig. 2. (Color online) (a) PL spectra of $In_{0.53}Ga_{0.47}As/In_{0.52}Al_{0.48}As$ modulation-doped quantum well, from 10 to 290 K. (b) PL decay time as a temperature for the transition at E1H1.

in energy-momentum phase space and spatially redistributed due to diffusion. In Fig. 2(b), the main decay time, τ_1, showed complicated variations at the lower T region but monotonically decreased at T larger than 90 K as the FES faded.

From these optical characteristics, we simplify the relationship of individual subband mobilities with relative PL intensities as a function of temperature. The diffusion length is given by $L = \sqrt{D\tau_R}$, where D is the diffusion coefficient that is related to the mobility μ using Einstein relation and τ_R is recombination lifetime. From this formalism without the carrier localization effects, Yablonskii*et al.* [28] reported an optical method for measuring L using one-dimensional diffusion. Correspondingly, I_{PL}- L relations can be adapted either as $I_{PL} \propto 1/L \approx 1/\sqrt{\mu\tau_R}$ with one-dimensional diffusion or as $I_{PL} \propto 1/(\mu\tau_R)$ with two-dimensional diffusion since L (~ 7.5 μm [29]) was considerably larger than the absorption length $1/\kappa$ (~ 0.2 μm at 514.5 nm [30]) in our structure. This approximation was employed for correlating I_{PL} with the individual subband electron mobilities, using the following three conditions: (1) The excess photo-carrier density was defined by the external excitation intensity that was negligibly smaller than the doping density. (2) The PL spectra exhibit three main peaks, among which I_{FES} is used as a normalization factor for subband intensities to avoid further complications by the hole localization effects compared to subbands. (3) The electrons in respective subbands have different mobilities

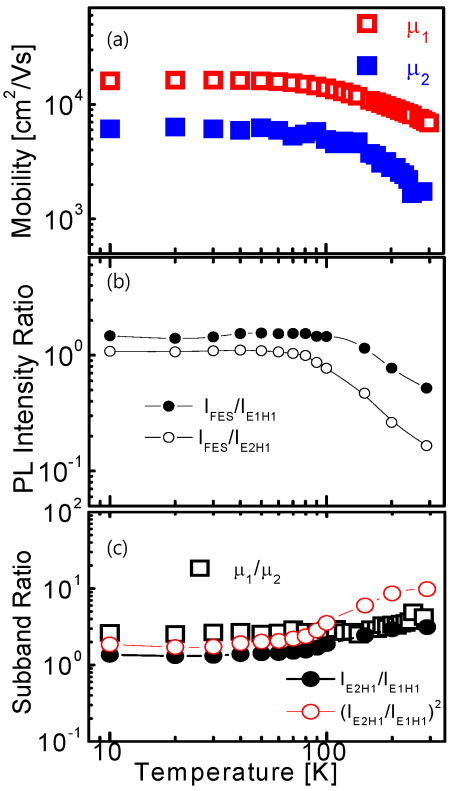

Fig. 3. (Color online) (a) Temperature-dependent subband electron mobilities; μ_1 and μ_2 are first and second subband mobilities, respectively, obtained from MSA. (b) Inverse PL intensity weighted by that at FES. (c) Comparison of mobility ratios with PL intensity ratios.

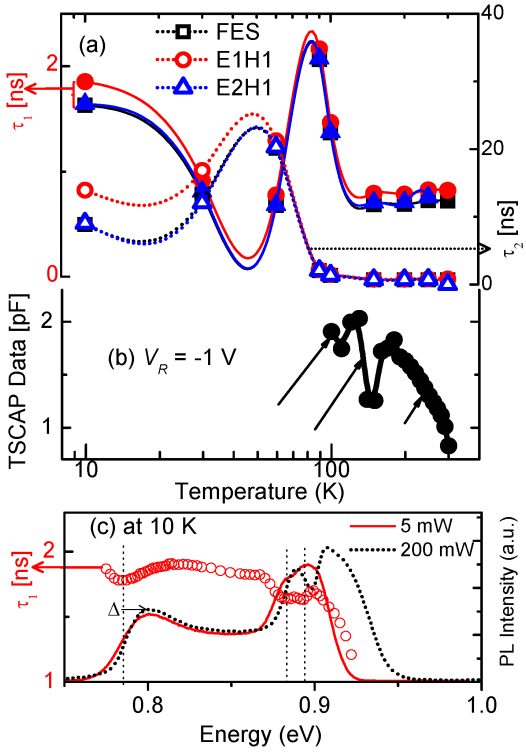

Fig. 4. (Color online) PL decay times at energy positions E1H1, E2H1, and FES as a function of temperature, taken from bi-exponential fittings.

because the Fermi momentum (k_F) of the first subband is larger than that of the second subband by the density-momentum relation $n = k_F^2/2\pi$, where the carrier density n is the essential element determining the electron mobility.

The assumptions above mean that excess electrons relax and contributes to the recombination at individual subband edges, and others recombine directly at localized hole-states from the Fermi sea, as shown in Fig. 1(b). These assumptions can be confirmed from the energy-dependent PL decay time in Fig. 4 because the PL decay time at E1H1 was slightly larger than that at E2H1.

Thus, we infer that the first and second electron subband mobilities (μ_1 and μ_2) are inversely proportional to either the PL intensity or square of PL intensities weighted by recombination times; that is, the subband-mobility ratio μ_1/μ_2 can be deduced either as

$$\mu_1(T)/\mu_2(T) = \frac{\tau_{E2H1}(T)}{\tau_{E1H1}(T)} \left(\frac{I_{\mathrm{E2H1}}(T)}{I_{\mathrm{E1H1}}(T)} \right)^2 \qquad (2)$$

in the case of one-dimensional diffusion or as

$$\mu_1(T)/\mu_2(T) = \frac{\tau_{E2H1}(T)}{\tau_{E1H1}(T)} \left(\frac{I_{\mathrm{E2H1}}(T)}{I_{\mathrm{E1H1}}(T)} \right) \qquad (3)$$

in two-dimensional diffusion. Equations (2,3) represent the electron mobilities in terms of PL peak in-tensities measured at a given temperature T. To obtain PL signatures of subband electron mobilities as a function of temperature, we determined PL peak intensities at positions E1H1, E2H1, and FES from Fig. 2(a). From equations (2,3), we compared the temperature-dependent mobilities for E1 (μ_1) and for E2 (μ_2) obtained from MSA with corresponding PL signatures in Fig. 3. First, the subband-specific mobilities [16] were defined as functions of temperature in Fig. 3(a). The subband carriers

at E1, whose scattering is affected by the alloy disorder, were found to dominantly contribute to the total carrier density and thus, resulted in μ_1 being quantified with the larger magnitude in the range of T. μ_2 was more strongly suppressed at elevated temperatures by optical phonon scattering. The detailed μ-T relationship follows from considering the alloy disorder, impurity scattering, and electron-phonon scattering [31]. The ratios of $I_{\rm FES}(T)/I_{\rm E1H1}(T)$ and $I_{\rm FES}(T)/I_{\rm E2H1}(T)$, considering that $I_{\rm FES}(T) \propto 1/\mu_{FES}$, $I_{\rm E1H1}(T) \propto 1/\mu_1$, and $I_{\rm E2H1}(T) \propto 1/\mu_2$ in lateral diffusion, are shown in Fig. 3(b). Comparing Fig. 3(a) and (b), we observe a similarity in T dependence, particularly at high temperatures, indicating the phenomenological correlation of transport phenomena with PL intensities in QW systems. Next, we compared the subband-mobility ratio of μ_1/μ_2 with the two-dimensional PL signature of $[I_{\rm FES}(T)/I_{\rm E1H1}(T)]/[I_{\rm FES}(T)/I_{\rm E2H1}(T)]$ and the one-dimensional $[I_{\rm FES}(T)/I_{\rm E1H1}(T)]^2/[I_{\rm FES}(T)/I_{\rm E2H1}(T)]^2$, weighted by recombination times (τ_{E1H1} and τ_{E2H1}), in Fig. 3(c). The one-dimensional PL intensity ratio (hollow circles) showed distinct behavior with μ_1/μ_2, whereas the two-dimensional PL intensity ratio (solid circles) merged into the mobility ratio at higher temperatures. This trend implies that the mobilities in QWs with many subbands can be analyzed using PL signatures for each subband, restrictively in systems with delocalized states.

PL signatures at low temperatures deviated from mobility ratio possibly using electronic localization, which was not considered in equations (2,3). However, the two-dimensional formula (solid dots) in Fig. 3(c) matched well with the mobility ratio $T > 100$ K, as the thermally activated carriers escaped the trap states situated inside the defects and impurities [32]. The inherent carrier localization in doped heterostructures can be manifested in the T-dependent decay time variations, as summarized in Fig. 4. The leading decay times τ_1 and adscititious values τ_2 were extracted for three main peaks, from fittings based on Eq. (1). For τ_1 and τ_2 at low T region (< 100 K $\equiv T_1^c$ for τ_1 and < 60 K $\equiv T_2^c$ for τ_2), the lowest energy state (E1H1) displayed a longer lifetime compared with higher energy states (FES and E2H1). This property is regarded as the characteristic of a localized effect [33]. Also, τ_i showed an abrupt variation around T_i^c, followed by exponential decrement and saturation with T at similar rates for all main peaks. This was anticipated for thermal activation and concomitant nonradiative recombination processes [34]. Therefore, T_1^c and T_2^c can be correlated with thermal activation energies for relatively shallower and deeper electron trap states [35], respectively, since the de-trapping temperature for holes should be higher than the reflection of T_2^c on the persistent emission features at FES in the entire T range of our sample. Such carrier delocalization at different T, distinguishing electrons from heavier holes, was previously reported from T-dependence of deep-level transient spectroscopy and thermally stimulated capacitance measurements in similar structures; in particular, the thermally stimulated capacitance data by raising T displayed two clear steps near T_i^c, ascribed to two electron trap levels whereas the hole de-trapping temperature was estimated to be larger than 200 K [16]. Thus, the abrupt changes of τ_i around T_i^c in Fig. 4 and the agreement between the mobility and inverse PL intensity ratios at higher temperatures in Fig. 3(c) implies that the individual subband scattering mechanism is influential for both mobilities and PL similarly, as long as the carriers are delocalized from trap states.

III. Conclusions

In this study, we investigated the correlation between mobilities and PL signatures in a 2DEG system with subbands by changing the temperature from 10–290 K in terms of an empirical optical model. The inverse ratio of subband PL intensities weighted by corresponding recombination times using spectrum- and time-resolved PL measurements matched well with the mobility ratio at the elevated temperature beyond 100 K as the electrons are thermally delocalized from the trap states and spatially distributed by lateral diffusion. Additionally, time-resolved PL was used to interpret the temperature-dependent carrier delocalization process at each subband and Fermi-energy. This work suggests that PL properties can further be used for identifying the scattering-mediated changes in mobilities and deepen insights into optical properties in various lowdimensional structures.

Acknowledgements

This research was supported by Basic Science Research Program through the National Research Foundation of Korea(NRF) funded by the Ministry of Science, ICT & Future Planning(2018R1A2B6008101) and the Ministry of Education(2021R1I1A2059710;2016R1A6A1A03012877; 2017R1D1A1B03032158;2021R1I1A1A01049157).

REFERENCES

[1] H. H. Choi *et al.*, Nat. Mater. **17**, 2 (2017) .
[2] M. Keever *et al.*, J. Appl. Phys. **53**, 1034 (1982) .
[3] H. A. Washburn, Thin Solid Films **45**, 135 (1977)
[4] G. Engels, J. Lange, Th. Schapers, and H. Luth, Phys. Rev. B **55**, R1958 (1997) .
[5] W. A. Beck and J. R. Anderson, J. Appl. Phys. **62**, 541 (1987).
[6] M. S. Skolnick *et al.*, Phys. Rev. Lett. **58**, 2130 (1987) .
[7] S. Rekaya, L. Sfaxi, C. Bru-Chevallier, and H. Maaref, Journal of Luminescence **131**, 7 (2011).
[8] C. Delalande *et al.*, Phys. Rev. Lett. **59**, 2690 (1987) .
[9] R. L. Weiher and W .C. Tait, Phys. Rev. B **5**, 623 (1972) .
[10] P. Irkhin and I. Biaggio, Phys. Rev. Lett. **107**, 017402 (2011) .
[11] S. Moritsubo *et al.*, Phys. Rev. Lett. **104**, 247402 (2010).
[12] T. Sogawa *et al.*, Phys. Rev. B **80**, 075304 (2009).
[13] S. Lou *et al.*, Sci. Rep. **5**, 14084 (2015) .
[14] H. Brugger, H. Müssig, and C. Wolk, Appl. Phys. Lett. **59**, 2739 (1991) .
[15] L. J. Cui *et al.*, J. Appl. Phys. **100**, 033705 (2006).
[16] I. H. Ahn, G. H. Song, and Y.D. Jho, Jap. J. Appl. Phys. **49**, 014102 (2010).
[17] R. A. Khabibullin *et al.*, Semiconductors **47**, 1215 (2013).
[18] P. W. Yu *et al.*, Appl. Phys. Lett. **65**, 3263 (1994) .
[19] D. Y. Lin, M. C. Wu, H. J. Lin, and J. S. Wu, Physica E **40**, 1757 (2008).
[20] J. S. Wu, C. C. Hung, C. T. Lu, and D. Y. Lin, Physica E **42**, 1212 (2010) .
[21] M. S. Skolnick, J. M. Rorison, K. J. Nash, and S. J. Bass, Surface Science **196**, 507 (1998)
[22] T. W. Kim, M. Jung, T. H. Park, J. Mat. Sci. Lett. **14**, 545 (1995)
[23] V. V. Solov'ev, I. V. Kukushkin, J. H. Smet, K. von Klitzing, and W. Dietsche, JETP Lett. **84**, 222 (2006).
[24] Y. D. Jho *et al.*, Phy. Rev. B **72**, 45340 (2005).
[25] S. Adachi, *Physical Properties of III-V Semicondutor Compounds* (Wiley, New York, 1992).
[26] H. Jeong *et al.*, Appl Phys. Lett. **100**, 092106 (2012).
[27] Y. D. Jho *et al.*, Phys. Rev. B **81**, 155314 (2010).
[28] G. P. Yablonskii textitet al., J. Cryst. Growth **275** (2005) e1733; K. V. Shalimova, Physics of Semiconductors, Energoatomizdat, Moscow, 1985, p. 392. (in Russian)
[29] R. Bhat, J. R. Hayes, H. Schumacher, M. A. Koza, D. M. Hwang, and M. H. Meynadier, J. Crystal. Growth. **93**, 919 (1988).
[30] D. Hahn *et al.*, J. Electron. Mater. **24**, 1357 (1995)
[31] I. H. Ahn and H. Joung, Jap. J. Appl. Phys. **49**, 084303 (2010)
[32] J. H. Song, *et al.*, Solid. State. Comm. **127**, 661 (2003).
[33] R. A. Mair, J. Y. Lin, and H. X. Jiang, Appl. Phys. Lett. **76**, 188 (2000) .
[34] Z. Su and S. Xu, Sci. Rep. **7**, 1 (2017)
[35] R. Murdey and N. Sato, Jap. J. Appl. Phys. **53**, 05FY04 (2014) .
[36] S. K. Brierley, J. Appl. Phys. **74**, 2760 (1993) .